Estimation of Water Cloud Properties from Satellite Microwave, Infrared and Visible Measurements in Oceanic Environments. I: Microwave Brightness Temperature Simulations

Bing Lin[1], Bruce Wielicki[2], Patrick Minnis[2], and William Rossow[3]
[1]Hampton University, Hampton, VA23668
[2]NASA Langley Research Center, Hampton, VA23681
[3]NASA Goddard Institute for Space Studies, New York, NY10025

Submitted to J. Geophys. Res.
Revised in September 1997

ABSTRACT

Theoretical calculations are used to examine the spectral characteristics of SSM/I (Special Sensor Microwave/Imager) brightness temperatures *Tb*s for non-precipitating clouds over oceans. It was found that liquid water path *LWP* and the cloud water temperature *Tw* could be derived simultaneously with a technique using the SSM/I 37- and 85-GHz brightness temperatures. Uncertainties in column water vapor *CWV* derived from 22-GHz data are the most important error sources in the estimation of *LWP* and *Tw*, while ice particles smaller than 100 μm in non-precipitating clouds have a very weak effect (< 1K) on the *Tb*s at the relevant SSM/I frequencies. When all SSM/I instrument noise and error sources associated with sea surface temperature, wind speed, and *CWV* are considered, the biases in *LWP* from current microwave methods are very small (≤ 0.01 mm) and the standard deviations vary from 0.02 to 0.04 mm. The *Tw* bias and standard deviation decrease with increasing *LWP* from about 6 and 8 K, respectively, for clouds with low *LWP* to < 1 K for *LWP* > 0.4 mm. For most marine stratocumulus clouds (*LWP* ~0.1 to 0.2 mm), the *Tw* bias and standard deviation are about 2 and 4 K, respectively, resulting in cloud height errors of ~1 to 2 km. The method should yield an improvement in the accuracy of retrieved *LWP* because it more closely approximates cloud temperature than previous techniques. To use the radiative transfer results, it is necessary to normalize or calibrate them to the observations. This relative calibration using 22-GHz brightness temperatures reveals differences of 2.86 K and -1.93 K for the 37-GHz horizontal and 85-GHz vertical channels, respectively, between the SSM/I observations and model simulations. In multi-layered cloud conditions, this new microwave analysis method, when combined with infrared data, should make it possible to determine cloud temperature for an upper-level ice cloud from the infrared brightness temperatures, while simultaneously deriving *Tw* and *LWP* for the lower liquid water cloud with the microwave data.

1. Introduction

Quantitative estimates of water cloud properties in marine environments using satellite measurements are critical to the assessment of global climate models. Water clouds not only affect fresh water transport by precipitation, which is one of the key factors determining oceanic thermohaline circulation, but also play a critical role in the radiative energy balance of the Earth/Atmosphere system (see *Wielicki et al.* [1995] for a recent summary). The Earth Radiation Budget Experiment (ERBE; *Ramanathan at al.* [1989]) and the International Satellite Cloud Climatology Project (ISCCP; *Rossow and Zhang* [1995]) have demonstrated the importance of clouds on the earth's radiation budget at the top of atmosphere and the surface. Changes in cloud vertical distributions and cloud particle phase can affect both shortwave and longwave radiation vertical profiles [*Gupta et al.* 1992; *Wielicki et al.* 1995], the vertical distribution of latent heat release, and cloud feedbacks in a changing climate [*Li and Le Treut* 1992]. Cloud vertical structure, i.e., cloud layering and overlap, is needed to help diagnose net surface longwave radiation and radiative divergence within the atmosphere from satellite measurements [*Charlock et al.* 1994]. Thus, monitoring of cloud layering and overlap is a critical component of any climate observing system.

In the tropics, thick anvil clouds cover large areas of the intertropical and southern Pacific convergence zones (ITCZ and SPCZ). Climatological observations report that about 40% of the clouds are multilayered in these regions [*Poore et al.* 1995; *Hahn et al.* 1982, 1984; *Warren et al.* 1985,1988]. In the midlatitudes, limited ship observations [*Hahn et al.* 1982] and studies of 3D Neph-analysis [*Tian and Curry* 1989] suggest that the frequency of stratus co-occurrence with high clouds is often greater than 50% over oceans. Because low overcast cases block most surface observations

and because of the sparse spatial coverage of observational stations, the estimated frequency for multilayered clouds has large uncertainties [*Poore et al*. 1995]. Satellite observations for multilayered clouds, at present, may be made in cases of thin cirrus over stratus by using infrared (IR) sounder data to determine the upper cloud level, and multispectral IR window channel data with spatial coherence methods to determine the lower level clouds [*Baum et al*. 1994]. Unfortunately there are almost no methods to estimate other types of multilayered clouds, especially if both layers are optically thick in visible (VIS) and thermal infrared wavelengths [*Wielicki et al*. 1995].

This paper and its companion discuss the estimation of cloud liquid water path (*LWP)* and temperature (*Tw*) of non-precipitating water clouds using combined passive IR, VIS and microwave (MW) satellite measurements. VIS and IR methods are used to discern clear and cloudy sky areas and to retrieve cloud-top temperature and optical thickness [e.g. *Rossow and Lacis* 1990 and *Minnis et al*. 1993], while the MW technique is used to estimate cloud liquid water path and temperature of water clouds even when they are obscured by high ice clouds.

Satellite MW measurements are commonly used to retrieve *LWP* over oceans [e.g. Petty 1990; *Greenwald et al*. 1993; *Liu and Curry* 1993; *Lin and Rossow* 1994]. Estimation of cloud water temperatures using passive MW data, however, has only been approached with methods that are basically empirical in nature and involve measurements at lower (< 40 GHz) frequencies [*Pandey et al*. 1983; *Liu and Curry* 1993]. Over ocean backgrounds, the brightness temperature *Tb* observed from space increases with increasing *LWP* and cloud height for lower microwave frequencies (see section 3). Thus, temperature signals from cloud liquid water can be confused with those from *LWP* limiting the use of lower frequency channels for estimating *Tw*. Using a microwave radiative transfer model (MWRTM), *Petty* [1990] found that the errors in estimated cloud heights, which are practically interchangeable with cloud temperatures, are about 80 to 100% of cloud height variations if the Special Sensor Microwave/Image (SSM/I) data are used alone, i.e., cloud height can not be reliably estimated. In his analysis, however, mean cloud height only varied from about 1 to 2.5 km depending on atmospheric profile, with a standard deviation equal to 60% of the value, i.e., the errors of cloud height estimates are around 0.6 to 1.5 km. The potential errors in cloud altitude estimation for higher clouds is unknown.

Furthermore, *LWP* is generally overestimated when derived with methods that implicitly or explicitly assume a fixed cloud temperature or fixed relationship between *Tw* and sea surface temperature and the actual cloud temperature is significantly colder than the assumed value [*Lin and Rossow*, 1994; *Liu and Curry*, 1993]. In the tropics, liquid water marine clouds can range from ~ -40 to almost 25°C. For example, if it is assumed that cloud water temperature *Tw* is 6°C colder than the surface [*Greenwald et al.,* 1993], midlevel supercooled clouds at -10°C would be ~30°C colder than the assumed cloud temperature over warm tropical seas at 28°C. Thus, a method that uses a value of *Tw* that is closer to the true value for a given retrieval should, on average, lead to more accurate values of *LWP*.

This paper takes a closer look at the potential for deriving *LWP* and *Tw* simultaneously using pairs of both low (37 GHz) and high (85 GHz) frequency SSM/I measurements. The primary objective of this study (Part I) is to develop a method for estimating the temperatures of low clouds, provide an improved estimate of LWP, and to understand the uncertainties in the retrievals. We will simulate the *Tb* signatures of SSM/I using a MWRTM and a full range of cloud temperatures (from surface to -40°C), analyze the variations of SSM/I *Tb* values as functions of *LWP* and *Tw*, discuss the sensitivity of microwave retrievals to instrument noise as well as to uncertainties in the major geophysical parameters affecting MW radiation over ocean surfaces, and perform a relative calibration of simulated brightness temperatures to SSM/I satellite observations. The companion paper (Part II) will propose a combined cloud *LWP* and *Tw* retrieval scheme based on the MWRTM calculated and calibrated lookup table for SSM/I *Tb*s, analyze observational *LWP* and particle size values, discuss the differences between cloud temperatures derived from IR and MW data, and investigate the retrieval of multilayered clouds. By combining MW remote sensing data with VIS and IR measurements in cases of non-precipitating multi-layered clouds, cloud top temperature of the upper ice layer can be measured using IR measurements, while the field-of-view average cloud temperature and liquid water path of the water cloud beneath the

ice can be determined from microwave measurements. This strategy would significantly improve the ability to quantify multilevel clouds over oceans.

2. Simulated Results

To understand SSM/I responses in oceanic environments, we numerically simulate the brightness temperatures of SSM/I at the top of atmosphere (TOA). SSM/I is a seven channel microwave radiometer that receives microwave radiation at frequencies of 19.35, 22.235, 37.0 and 85.5 GHz (hereafter referred to as 19, 22, 37 and 85 GHz for brevity). Vertical (v) and horizontal (h) polarization measurements are taken at all frequencies, except at 22 GHz for which SSM/I measures only vertical polarization. The view angle of SSM/I on the earth is nearly constant at approximately 53 degrees. Although there are theoretical studies on microwave radiation for non-precipitating clouds [e.g., *Petty and Katsaros* 1992 and 1994], accurate relationships of the response of SSM/I to several geophysical variables are still under study. For example, the variations of brightness temperature with cloud liquid water temperature and liquid water path at 85 GHz are usually not similar to those at lower frequencies.

The model used to simulate SSM/I Tb values is a plane-parallel MWRTM [*Lin and Rossow*, 1997; *Lin* 1995] that is essentially the same as those of *Wilheit et al.* [1977], *Yeh et al.* [1990] and *Liu and Curry* [1992]. The absorption, scattering, and extinction coefficients and phase functions are calculated according to Mie theory. The complex refractive indices of ice are taken from the tables of *Warren* [1984]. There are basically two available methods to obtain the refractive indices of liquid water droplets: the empirical formulae of *Ray* [1972] and the model of *Liebe et al.* [1991]. For SSM/I frequencies, the relative differences of the absorption coefficients of water particles calculated from *Ray* [1972] and from *Liebe et al.* [1991] are generally very small (<5%) when water temperature is above freezing point. For supercooled water, the differences can be large (>15%). It is unknown which one is more realistic because both *Ray* and *Liebe et al.* do not have enough measurements to support their modeling efforts for cold (< 0°C) water temperatures. We use empirical formulae of *Ray* [1972] following *Smith et al.* [1992]. The *Liebe* [1985] model and *Petty* [1990] method are employed to specify atmospheric gas absorption and sea surface emissivity, respectively, with a near-sea-surface wind speed WS of 7.5 m/s. The atmospheric temperature and gas abundance profiles are taken from climatological profiles for tropical, midlatitude summer, midlatitude winter, and US standard atmospheres [*McClatchey et al.* 1972]. The surface temperatures for these profiles are approximately 26, 21, -1 and 15 °C, respectively, and represent a wide range of conditions for ocean backgrounds.

Because the focus is on non-precipitating clouds, all water droplets are assumed to be smaller than 100 μm. In this case, the dominant microwave radiative process within water clouds is absorption [*Petty* 1990 and references therein]. For non-precipitating ice clouds with similarly sized particles, both scattering and absorption are negligible. Therefore, we do not include ice clouds at the present stage and will discuss them later. To illustrate the variability of the LWP and Tw effects on microwave radiances, we use four different liquid water cloud heights in all four atmospheric profiles. These low, lower-middle, upper-middle, and upper-level clouds are all assumed to be 0.5-km thick. Thus, the liquid water content in each cloud increases with LWP. The corresponding heights for the clouds depend on the atmospheric profiles and are about 2, 4, 6 to 7, and 7.5 to 10.5 km respectively, as listed in Table 1. The higher clouds represent supercooled liquid water clouds, which have been frequently observed [*Feigelson* 1978; *Hobbs and Rangno* 1985; *Sassen et al.* 1989]. The cloud temperature at upper levels is about -40 °C, the expected limit for supercooled water clouds.

The simulated SSM/I responses for low level clouds (figure 1), which are similar to those of *Petty* [1990], are shown for the tropics (Fig. 1a), midlatitude summer (Fig. 1b), midlatitude winter (Fig. 1c), and the US standard atmosphere (Fig. 1d, hereafter all figures have the same order unless specified otherwise). In clear-sky cases (LWP = 0), all brightness temperatures are very cold (less than 250 K for lower frequencies) due to the low sea surface emissivity of about 0.5 [*Petty* 1990; *Petty and Katsaros* 1994]. Vertically polarized brightness temperatures (solid curves) are usually greater than the corresponding horizontally polarized values (broken curves) because sea surface emission is stronger in the vertically polarized direction [*Petty*, 1990; *Petty and Katsaros* 1994]. The values at 22 GHz (dotted curves) is typically

used to estimate column water vapor (*CWV*), especially in clear sky cases (cf., section 5) because the channel is centered on a weak water vapor absorption line. Thus, the following discussion of *Tb* variations for liquid water clouds concentrates on the other frequencies.

Brightness temperatures at all SSM/I frequencies, especially at 19 and 37 GHz, increase with increasing *LWP* when it is less than 0.5 kg/m^2 (or 0.5 mm). This nearly linear behavior arises because low-level clouds are physically warmer than the brightness temperatures of the radiance emitted from the surface and atmosphere below the clouds and their total MW absorption optical depths are small. These features serve as the physical basis for using empirical and/or simplified physically-based retrieval methods to estimate *LWP*. Figure 1 also shows that the 37-GHz channels, especially 37h, typically have a stronger dependence of *Tb* on *LWP* than the other channels, i.e., they are more sensitive to variations in cloud liquid water. Based on their sensitivity to *LWP*, along with a relatively low sensitivity to *CWV* (see section 4), the 37-GHz channels, especially 37h, are most frequently used to estimate *LWP*.

The microwave absorption coefficients of liquid water increase with decreasing cloud water temperature, while the cloud physical temperature is usually warmer than the microwave brightness temperature at low frequencies. Thus, the brightness temperatures of higher altitude liquid water clouds (Fig. 2) are often greater than the *Tbs* of lower clouds, especially at 19 and 37 GHz (cf., Figs. 1 and 2). The steeper slope of *Tb* as a function of *LWP* in figure 2 compared to that in figure 1 clearly reflects that the absorption coefficients of colder clouds are greater than those of warmer ones (see also Figs. 3 and 4). Because both increasing *LWP* and cloud height can produce greater radiances at 19 and 37 GHz, the signals from cloud liquid water temperature can be confused with those from *LWP*. These effects limit the use of lower frequency channels for estimation of cloud temperature [*Lin and Rossow* 1994; and references therein]. At 85 GHz, the situation is different; the *Tb*s may even decrease with increasing *LWP*, especially for vertically polarized *Tb*s (compare Fig. 2 with Fig. 1). Although the 85-GHz absorption coefficients still increase with decreasing cloud temperature as at lower frequencies, the sign of the change in *Tb* with *LWP* depends on the competition between cloud temperature and upwelling microwave radiation at cloud base. The absorption coefficients only affect the rate of change of *Tb*s with *LWP*, not the sign.

To determine the variation of MW radiation with cloud water temperature, we examine the *Tb* results for all four cloud-height cases. Figure 3 shows the horizontally polarized 19- and 37-GHz brightness temperatures at the top of the atmosphere (TOA). Vertically polarized *Tb*s (not shown) have similar features. As expected, the *Tb*s at both frequencies increase as *LWP* and cloud height increase. The range in *Tb* differences between the various cloud levels is greater for the warmer atmospheres than for the colder profiles primarily because of the larger potential range in *Tw* in warmer climates (i.e., there are larger temperature differences from the surface to about -40 °C in warmer climates than for colder climates). For a given *Tb* at either 19 or 37 GHz, there are multiple solutions for *LWP* as a function of varying cloud temperature (or height). Furthermore, the *LWP* errors produced by incorrectly accounting for *Tw* in one channel, say 37h, cannot be determined with the other channel. The variations of *Tb* with *LWP* and *Tw* in these two channels are very similar, especially when *LWP* is less than about 0.5 mm, a range that includes most non-precipitating clouds. Thus, it is impractical to estimate cloud temperature using only the lower-frequency channels [*Lin and Rossow* 1994 and references therein].

Figure 4 shows the vertically polarized *Tb*s at 37 and 85 GHz for the same conditions used in figure 3. By comparing to figure 3, it is clear that the Tb_{37v}'s have features similar to Tb_{37h}, except that the Tb_{37v}'s are larger, much less sensitive to *Tw*, and somewhat less sensitive to *LWP* than Tb_{37h},. Unlike the lower-frequency *Tb*s, Tb_{85v} may increase or decrease with increasing *LWP* depending on the difference between *Tw* and the brightness temperature from emission below the clouds, as mentioned earlier. Moreover, for the same *LWP*, Tb_{85v} for all four climatic profiles decreases with increasing cloud height, i.e., the higher the clouds, the colder the brightness temperatures. Comparing the values of *Tw* - *Tb* between warmer and colder clouds, we find that the values are small or even negative in colder clouds and the changes in liquid water absorption coefficients at 85 GHz as a function of cloud temperature only affect the relative magnitude of

the *Tb* changes. Thus, in the competition between the effects of changing water absorption coefficient and cloud temperature on TOA brightness temperature, the latter dominates. These two factors (the temperature difference and water absorption coefficient) enhance the depression of Tb_{85v} when *Tw - Tb* is less than zero, or when the clouds are very cold (cf., Fig. 4). This result demonstrates that the dependence of Tb_{85v} on *Tw* has a sign opposite that for the lower frequencies.

As a result, we propose to estimate *LWP* and *Tw* simultaneously using SSM/I measurements at 37 and 85 GHz. We use the observed *Tb*s at 37 and 85 GHz as input for our calculated SSM/I *Tb* lookup table, and then search for the best match between the observed and simulated *Tb*s to obtain simultaneous estimates of *LWP* and *Tw*. Because most clouds are not optically thick at these wavelengths, *Tw* represents a liquid-water-content-weighted temperature averaged over the water cloud layer. The detailed retrieval scheme is discussed in Part II of this series of papers [*Lin et al.* 1997]. This method generally can be used for single layered, non-precipitating water clouds. For multilayered, non-precipitating water clouds, because Tw values are the averages for water cloud layers, the cloud height estimates can be different from the real clouds. The 85h *Tb*s (not shown here) are similar to those at 85v *Tb*s, except that they do not depend as strongly on *LWP* and *Tw* for the coldest clouds.

The decrease in *Tb* with increasing cloud height at 85 GHz is similar to brightness temperature variations at thermal IR wavelengths. There are several differences, however, between thermal 85-GHz microwave and IR radiation:

1). The *Tb*s at thermal IR wavelengths are usually determined by cloud top temperature and are relatively insensitive to *LWP*, since most water clouds have emissivity near 1 (*LWP* > 0.05mm). For thermal radiation at 85 GHz, the optical thickness for the majority of non-precipitating clouds (*LWP* < 0.5 mm) is less than 1 [*Petty and Katsaros* 1992], i.e., the *Tb*s at TOA are strongly affected, not only by *Tw*, but also by *LWP*, CWV, sea surface temperatures *SST*, and *WS*.

2). Thermal IR *Tb*s typically decrease monotonically with increasing cloud height and *LWP* if clouds are very thin. The 85GHz *Tb*s may increase or decrease with *LWP* depending on both *Tw* and *Tb*, which varies strongly with *CWV* and surface emissivity.

3). Thermal IR *Tb*s are very sensitive to ice cloud, while non-precipitating ice cloud has very little effect on MW radiation, especially at the SSM/I frequencies as demonstrated in the following section.

The first two differences listed above indicate that cloud temperatures estimated at IR wavelengths will more closely approximate cloud-top temperature, while *Tw* estimated at microwave wavelengths will more closely approximate a layer average cloud temperature. The third difference suggests that the MW measurements can be used to estimate the height of a liquid water cloud layer beneath a cirrus layer, even if the cirrus layer were optically thick in the thermal IR. In this manner, the IR data could be used to determine cloud-top temperature (or altitude) of the upper cloud layer, while the MW data determine the height of the liquid-water cloud beneath the cirrus.

3. Sensitivity Test

To understand the effects of geophysical parameters on microwave radiation and to predict the accuracy of any resulting *LWP* and *Tw* retrievals, we simulate the SSM/I *Tb* uncertainties associated with the potential errors in sea surface temperature, wind speed, column water vapor, and scattering by ice particles. *Lin and Rossow* [1994] examined a similar problem using a simplified microwave radiative transfer method. In their results, they concentrated on lower frequencies using observed SSM/I data. Here we will extend those results to include the SSM/I high frequency channels and to theoretically investigate the effects of ice scattering. We first focus on the *Tb* sensitivities of low and lower middle-level clouds since many water clouds are below about 4 km, then provide an error analysis on *LWP* and *Tw* estimates in terms of multi-channel and multi-dimensional error dependencies.

The theoretical calculations show that for the lower middle-level clouds in a midlatitude summer climatological profile, the changes of the Tb_{37v} and Tb_{37h} change with *LWP* by about 0.5 K and 1 K per 0.01 mm, respectively. The lower sensitivity of the vertical polarization results from the smaller temperature differences between cloud water and the microwave radiation (i.e., $|Tw - Tb_{37v}| < |Tw - Tb_{37h}|$). At 85 GHz, the v and h *Tb* vary with cloud temperature by about 1.4 K and 1 K per 1 °C per 1 mm, respectively. The larger the *LWP*, the greater the

sensitivity of *Tb* to changes in *Tw* (cf., Fig. 4). The total errors in microwave-estimated *LWP* and cloud temperature are primarily caused by the SSM/I multi-channel noise and uncertainties in the retrieval inputs (such as *CWV*, *WS* and *SST*).

To provide sensitivity tests of individual error sources, all geophysical parameters, except the parameter being tested, used in the microwave radiative transfer model are fixed at the values discussed in the previous section. We then determine the TOA brightness temperature errors that would result from an uncertainty in the tested parameter. Due to the similarity between vertical and horizontal brightness temperatures, the results are only shown for the horizontal polarization case.

Figure 5 shows the absolute value of the *Tb* error caused by an error *DTb* of ± 2K in *SST* (Fig. 5a) and by an error of ± 2 m/s in the near-surface windspeed (Fig. 5b). Results are given for the midlatitude summer climatological profile. The assumed errors in *SST* and *WS* are representative of current remote sensing algorithm accuracies [*Rossow and Garder* 1993; *Goodberlet et al.* 1990].

Figure 5a shows that the *Tb* uncertainties in caused by 2K errors in *SST* are usually less than 1K, the level of SSM/I instrument noise. Given the sensitivity of *LWP* to *Tb*, this result indicates that *SST* errors are a minor source of error for determination of *LWP* or *Tw*. For the uncertainties in *WS*, the *Tb*s at 85 GHz are within the instrument noise level, but the *Tb*s at lower frequencies are in error by 2 - 3 K, which is significant for *LWP* estimation. The unequal absolute value of *DTb* between the +2m/s *WS* and -2m/s *WS* errors shown in figure 5b are produced by the non-linear relationship between sea surface emissivity and near-surface wind speed. Since the climatological near-surface wind speeds are about 3 to 10 m/s, this nonlinear behavior will cause a bias in retrieved *LWP* even if *WS* errors are random and unbiased [cf., *Lin and Rossow* 1994].

The effect of errors in *CWV* for all four climatological atmospheric profiles are shown in figure 6. *CWV* errors are assumed to be ±10%. Given 10% relative error, the absolute *CWV* error in the tropics and the summer midlatitudes is about 3 - 4 kg/m^2, which is the current level of uncertainty for microwave remote sensing of *CWV* [*Sheu and Liu* 1995]. Other studies [e.g., Petty 1990] have claimed much smaller (about 1.5 - 2 kg/m^2) errors in estimated CWV. As shown in Fig. 6, the resulting *Tb* errors (about 3 K or larger at 19 and 37 GHz) are significantly greater than those found for *SST* or *WS*. An exception occurs for the midlatitude winter profile which has a small *CWV* amount (about 8.5 kg/m^2) and, therefore, much smaller absolute errors in *CWV*. The errors at 85 GHz rapidly decrease with increasing *LWP* because liquid water absorption and emission are much stronger at 85 GHz than at the lower frequencies. Figure 6 indicates that the uncertainties in *CWV* are the most important source of error in estimating *LWP*, especially at lower frequencies, as discussed by *Lin and Rossow* [1994]. The 37 GHz channels show less sensitivity to *CWV* errors than 19 GHz for all values of *LWP*, and are less sensitive than 85 GHz for small values of *LWP*. This is one of the reasons for using the 37 GHz *Tb*s to estimate *LWP*. If the *CWV* errors at 37 GHz are converted to equivalent errors in retrieved *LWP*, the resulting uncertainty in *LWP* is about 0.05 mm, similar to the values given by *Lin and Rossow* [1994]. More accurate *CWV* values are required not only for studies of water vapor, but also for methods that utilize passive microwave radiances to estimate cloud *LWP*. While the current approach is different, the above sensitivities to *SST*, *WS*, and *CWV* are consistent with those from *Lin and Rossow* [1994]. For LWP < 0.2mm, the errors (about 3 to 7 K) at 85 GHz caused by *CWV* uncertainties are much larger than SSM/I instrument noise. These errors may cause large errors in cloud water temperature estimates if only the 85 GHz channel is used in the retrieval. When *LWP* and *Tw* are estimated simultaneously, most *Tb* errors caused by *CWV* are canceled by similar *Tb* errors in *LWP* estimates using 37 GHz. Thus, the errors in *Tw* estimates are reduced (see results below and cf., Figs. 9 and 10).

To consider the effect of ice clouds on microwave radiation, we place an ice cloud layer above the top of a lower middle level liquid water cloud layer. The two layer cloud cases use the summer midlatitude climatological profile. Results for other water cloud levels and climatological profiles are similar. Figure 7 shows the effects of ice scattering on TOA *Tb* changes for ice clouds composed of 40 μm radius spheres (Fig. 7a) and 100 μm spheres (Fig. 7b). Brightness temperature changes are small at all frequencies (less than 1 K), even for extremely thick ice clouds (*IWP* = 0.6 and 0.9 mm). In general, the effect of the ice-cloud layer

increases with frequency and with particle size. Ice absorption at MW wavelengths is very low due to the minimal imaginary part of the refractive index for ice [*Warren* 1984]. The scattering effects of small ice particles (radius less than 100 μm) are also negligible because the particle size parameter is much less than one, even at 85 GHz. Thus, non-precipitating ice clouds usually are not detected by current microwave instruments. With increasing ice crystal size, scattering effects become more important, especially at 85 GHz.

Figure 8 gives results for 500 μm radius ice particles for the same conditions used in figure 7. In this case, the scattering effects are large at 85 GHz (Fig. 8c). Ice scattering effects at 85 GHz depend strongly on *IWP* (10 to 30K) and less on the upward emission of microwave radiation by the sea surface and liquid cloud layer below (hence the dependence on *LWP* shown in Fig. 8c). The effect of ice scattering is small at 37 GHz for most liquid water clouds (Fig. 8b, less than 1K for $LWP < 0.5$ mm) and probably undetectable at 19 GHz (Fig. 8a; notice the scale differences among the three panels). The reduced scattering effects at 37 and 19 GHz are caused by the decreasing particle size parameter at the lower frequencies.

The above sensitivity tests suggest that most non-precipitating ice clouds have minimal effect at 19 through 85 GHz. As a result, by combining IR and MW satellite measurements, we can expect to estimate the temperatures of both an overlapped ice cloud layer (using IR) and water cloud layer (using MW) with reasonable accuracy for most cases of overlapped cloud over ocean. Exceptions include ice clouds with both very large particles and large *IWP*, or cases of very low *LWP* (< about 0.04 mm; see discussions later).

In order to test *LWP* and *Tw* estimates for microwave methods in terms of multi-channel and multi-dimensional error dependencies, we simulate the complete microwave retrieval processes. Because ice clouds have very weak effects on microwave radiation, the following simulation assumes $IWP=0$. The actual simulation procedure is:

1) *for a given climatological profile, obtain initial values of SST_0, WS_0, CWV_0, LWP_0 and Tw_0;*
2) *calculate brightness temperatures at TOA using MWRTM for each relevant channel;*
3) *add instrument noise to the calculated brightness temperatures to simulate SSM/I Tbs;*
4) *add errors to the original values of SST_0, WS_0, and CWV_0 to obtain simulated inputs of SST, WS, and CWV;*
5) *retrieve LWP and Tw values using SST, WS, and CWV from step 4 and Tbs from step 3;*
6) *repeat steps 3 to 5 100 times for each value of LWP_0 and Tw_0 in order to have enough data for stable statistics.*

Here, we assume all error sources are Gaussian random variables. The SSM/I instrument noise levels obtained by *Hollinger et al.* [1990] are used as the standard deviation (or σ) in the simulation. Due to field of view (FOV) differences between 85 GHz and other channels (four to one), averaged *Tb* values at 85 GHz are used for each pixel at lower frequencies. Because the size of marine stratiform clouds is generally > 50km [*Tian and Curry*, 1989; *Liao et al.* 1995] and adjacent clouds tend to locate in the same level, the effect of the remain FOV differences between 37 and 85 GHz on LWP and Tw retrievals is minimal for these clouds. For broken clouds, this effect produces random errors that can be small in the averages. As discussed before, the errors in *SST* and *WS* are 2 K and 2 m/s, respectively. Because *CWV* is the most important error source (Fig. 6 or *Lin and Rossow* [1994]), we use averaged *CWV* retrievals to reduce random errors. This study and its companion use an average of four adjacent *CWV* values as input to estimate *LWP* and *Tw* values. If it is assumed that the uncertainties in the four values of *CWV* used in the pixel averaging are uncorrelated then it can be concluded that the errors in *CWV* are about half of the uncertainties discussed earlier (i.e., 5%). Although this assumption may not be valid in all cases, it yields a *CWV* uncertainty comparable to that given by *Petty* [1990] for *CWV*.

While the details of the *LWP* and *Tw* retrieval scheme are discussed in the companion paper, a brief overview is given here. IR and MW remote sensing measurements are the primary inputs for the retrieval algorithm. *SST* and cloud top temperature are estimated from IR measurements, while *WS* and *CWV* are MW retrievals. For a given set of these parameters and the SSM/I *Tb*s (here, all *Tbs* are simulated values with Gaussian instrument noise), the scheme automatically searches for the best

solution from cloud top down to the surface according to a MWRTM-produced lookup table. Due to monotonic functions of *Tb37* and *Tb85* on *LWP* and *Tw* (cf. figures 3 and 4), current method has unique solution.

Figures 9 and 10 are the simulated results of *LWP* and *Tw* biases and standard deviations for the tropical and midlatitude winter profiles, respectively, which represent the extreme conditions in this analysis. The patterns of the parameter bias and standard deviation in both figures are more or less similar. However, the magnitudes of the errors for midlatitude winter are much smaller because of the reduced absolute *CWV* uncertainties. Thus, we will focus on the worst case scenarios exemplified in the tropical results.

In figure 9, the *LWP* biases (upper left panel of Fig. 9) are mostly within $\pm$0.01 mm of the reference values, especially for *LWP* less than 0.5 mm (i.e., for most non-precipitating clouds). The standard deviation of the *LWP* error (upper right panel of Fig. 9) decreases from about 0.04 mm for warm clouds to about 0.02 mm for cold clouds due to the temperature dependence of liquid water absorption.

The bias and standard deviation of *Tw* errors (lower panels of figure 9), decrease with increasing *LWP* from values of about 6 and 8 K, respectively, to < 1 K. For most marine stratocumulus clouds (*LWP* about 0.1 - 0.2 mm), bias error is about 2 K with standard deviation about 4 K, which is basically consistent with the estimate from *Petty* [1990]. When cloud *LWP* increases, radiation emitted from clouds at 85 GHz dominates over that from the surface and from the atmospheric gases. As a result, the error in *Tw* decreases with increasing *LWP*. This result suggests that the uncertainty in microwave-estimated cloud height is about 1-2 km for most liquid water clouds.

Current retrieval technique should obtain more accurate *LWP* values than those estimated from the methods that implicitly or explicitly assume a fixed cloud water temperature or fixed relationship between *Tw* and *SST* when the actual cloud water temperature is considerably colder than the assumed value. Figure 11 shows the simulated bias and standard deviation values of *LWP* estimates for tropical (upper panels) and midlatitude winter (lower panels) profiles. All simulating processes are the same as those done for figures 9 and 10 except using a cloud water temperature equal to *SST-6* [*Greenwald et al.* 1993] during retrieving *LWP*. Although the *LWP* standard deviations in figure 11 only slightly larger than those in figures 9 and 10, the bias errors (all positive) are much larger (notes the scale difference between Fig. 11 and Figs. 9 and 10), especially for tropical cases. For example, the errors can be as large as about 0.15 mm for a tropical cloud with LWP = 0.1~ 0.2mm and Tw=-10°C. Even for tropical warm clouds, the biases could be about a factor of 2 larger. Also, the thicker the clouds the bigger the positive biases because generally, the *LWP* errors caused by *Tw* errors are proportional to the products of the relative errors of cloud absorption coefficients (which can be 100% for temperature range from -20 to 20 °C, cf. *Liu* and *Curry* [1993]) and *LWP* values. These results illustrate that the combined retrieval of *LWP* and *Tw* may reduce the errors in *LWP* by about a factor of 2 because it could yield a temperature that is closer to the true cloud temperature than assumed in most microwave *LWP* retrievals.

4. Calibration

In order to use the model-simulated results to estimate geophysical parameters (*LWP* and *Tw*), we need to calibrate the radiative model *Tb* values to be consistent with SSM/I measurements. Because many factors affect *Tb* values for cloudy sky cases, we choose clear-sky data to test the differences between model results and microwave observations. Microwave data from SSM/I on the satellite of the Defense Meteorological Satellite Program, F-11, are used here. For this purpose, visible and infrared measurements from the Meteosat at 0° longitude are collocated with SSM/I data to within $\pm$15 minutes. The Meteosat data were taken during the Atlantic Stratocumulus Transition Experiment (ASTEX) during July 1992 for a region of the Atlantic covering 25° to 40° N and 330° to 345°E. The bispectral threshold technique of *Minnis et al.* (1987; 1992) was used to retrieve cloud cover, optical thickness, cloud top temperature, and *SST* in each 0.5° grid box. Clear sky is defined, using the Meteosat analyses, as zero cloud cover within a grid box. This definition avoids cloud contamination produced by the low spatial resolution of the SSM/I. Near-sea-surface windspeeds are estimated from SSM/I data using the method defined by *Goodberlet et al.* (1990).

Given *SST* from Meteosat and *WS* from SSM/I, *CWV* is the major uncertainty in determining clear-sky brightness temperatures.

In this case, 22 GHz *Tb*s are used as a base line to inter-calibrate model-simulated and SSM/I-observed brightness temperatures.

The model results and SSM/I measurements are compared as follows:

1) *Simulate SSM/I Tbs according to the estimated SST and WS and a given minimal CWV value of 5 kg/m^2.*
2) *Compare model-simulated Tb with SSM/I observations for the 22 GHz channel. If the model Tb is less than the observation, increase CWV until the simulated 22v Tb is equal to the SSM/I observed value. In this step, clear sky CWV values are estimated as side products.*
3) *Check the differences in the observed and simulated Tbs for the 19, 37 and 85 GHz channels.*

The advantage of this procedure is that the biases in the other channels, especially in the 37h and 85v channels used for *LWP* and *Tw* estimation, can be easily estimated. The disadvantage is that the absolute biases between the 22v channel and all other frequencies and polarizations are lost. In that sense, the current calibration is only relative and is specific to the particular radiative model and the SSM/I sensor.

Figure 12 gives the *Tb* difference between SSM/I observations and model simulations for 37h (left panel) and 85v (right panel) channels. The test gives biases for the 37h and 85v channels of about 2.86 K and -1.93 K, respectively. The biases in other channels are similar in magnitude. Although these values are relatively small (less than 2%), they are not negligible for physical retrievals (cf., last section). *Greenwald et al.* [1993] found a similar bias of 3.58K for the SSM/I 37 GHz channels. Others [cf., *Petty* 1990] also find small differences between model-simulated and SSM/I-observed *Tbs* at all SSM/I frequencies. These small biases could be produced by either uncertainties in the microwave radiative transfer models or by small errors in SSM/I instrument calibration.

Although we can not estimate bias in the 22 GHz channel, we can estimate its direct effect by estimating *CWV* retrievals. Figure 13 compares the model *CWV* estimates with the values retrieved from the *Schluessel and Emery* [1990] scheme (hereafter SE). The SE scheme is used because its retrievals were shown to have a high correlation coefficient (0.75) and small root mean squared error (5.31 kg/m^2) when compared with radiosonde data [*Sheu and Liu* 1995]. Our comparison shows that the current results are well correlated with the SE method (a correlation coefficient of about 0.98) with a relatively small bias of 4.39 kg/m^2. The linearity in figure 13 is a result of the primary use of the 22 GHz channels in both the SE method and the current approach, as well as the fact that the 22 GHz channel is not saturated for water vapor levels typical of the ASTEX data.

In summary, clear sky calibration tests suggest that the radiative model is consistent with the SSM/I observations. The differences between the two are small, but not negligible for physical retrievals. Studies should be directed at further reducing these differences.

5. Summary

Simulated SSM/I brightness temperature values are significantly affected by both cloud water path and temperature and usually increase with increasing *LWP* for warm non-precipitating clouds in oceanic environments. Unlike lower frequency channels, the brightness temperatures at 85 GHz do not increase, but decrease with decreasing cloud water temperature. The relationship between 85 GHz *Tb* and *LWP* is complicated by the fact that the brightness temperatures at this frequency can increase or decrease with increasing *LWP* depending on the difference (or competition) between *Tw* and the upwelling radiance at cloud base. It has been shown that the different dependencies of 37 and 85 GHz radiation on cloud temperature can be exploited to estimate *LWP* and *Tw* for liquid water clouds simultaneously using SSM/I brightness temperatures at those frequencies.

Sensitivity tests show that *CWV* uncertainties are the most important error source for *Tb*, *LWP* and *Tw* estimation while non-precipitating ice clouds have little effect on SSM/I *Tb* values. Thus, by combining microwave with IR remote sensing for non-precipitating clouds, it should be possible to determine the cloud temperature for both an upper ice particle cloud layer using the IR sensor, while simultaneously deriving cloud temperature and *LWP* for a lower liquid-water layer, even when optically thick ice clouds are present.

When all SSM/I instrument noise, *SST*, *WS*, and *CWV* error sources are considered, we find that the biases in cloud *LWP* estimates for current microwave methods are very small

(within 0.01 mm), while standard deviations are about 0.02 - 0.04 mm depending on cloud temperature. The *Tw* bias and standard deviation decrease with increasing *LWP* from about 6 and 8 K for clouds with small *LWP* to less than 1 K for *LWP* > 0.4 mm. For most marine stratocumulus clouds (*LWP* ~ 0.1 to 0.2 mm), the *Tw* bias error is about 2 K and the standard deviation is 4 K. This result shows that cloud height estimated using these microwave methods will have an uncertainty of about 1-2 km. While these errors may be relatively large compared to those for IR retrievals of cloud height for unobstructed low clouds, they represent a dramatic improvement for estimating the height of the lower cloud in overlapped conditions. Furthermore, the combined retrieval of *Tw* and *LWP* may reduce the error in *LWP* by about a factor of 2 because it could yield a temperature that is closer to the true cloud temperature than assumed in most microwave *LWP* retrievals.

Due to relatively strong water vapor absorption at 22 GHz, the brightness temperatures at this frequency are used to calibrate the radiative-model-simulated results and to estimate column water vapor. This relative calibration shows that there are small, but not negligible differences between SSM/I observations and model simulations. By applying this calibration to each dataset, it will be possible to apply the technique developed here to any SSM/I dataset taken over ocean.

Acknowledgments

This research is part of the studies of the Clouds and the Earth's Radiant Energy System under the NASA Earth Observing System and the First ISCCP Regional Experiment. One of the authors (BL) gratefully acknowledges support from NASA under contract NAS1-19656. Some of the satellite data analyses were supported by the Office of Naval Research through R. F. Abbey under Grant USN-N0001491IMP24011. The DMSP data were provided by the Distributed Active Archive Center at the NASA Marshall Space Flight Center in Huntsville, Alabama. F. Wentz of Remote Sensing Systems in Santa Rosa, California supplied the algorithms for reducing SSM/I antenna temperatures. The 1992 Meteosat data were purchased from the European Space Agency with the assistance of Genevieve Seze of the Laboratoire Meteorologie Dynamique in Paris, France.

References

Baum, B.A., R.F. Arduini, B.A. Wielicki, P. Minnis, and S.C. Tsay, Multilevel cloud retrieval using multispectral HIRS and AVHRR data: nighttime oceanic analysis, *J. Geophys. Res*. **99**, 5499-5514, 1994.

Charlock, T., F. Rose, T. Alberta, G. L. Smith, D. Rutan, N. Manalo-Smith, P. Minnis, and B. Wielicki, Cloud profiling radar requirements: Perspective from retrievals of the surface and atmospheric radiation budget and studies of atmospheric energetics. Utility and Feasibility of a Cloud Profiling Radar, WCRP-84, IGPO Publication Series No. 10, January, B10-B21, 1994.

Feigelson, E.M., Preliminary radiation model of a cloudy atmosphere, Part I. Structure of cloud and solar radiation, *Beitr. Phys. Atmos*., **51**, 203-229, 1978.

Goodberlet, M.A., C.T. Swift, and J.C. Wilkerson, Ocean surface wind speed measurements of Special Sensor Microwave/Imager (SSM/I), *IEEE*, **GE-28**, 832-828, 1990.

Greenwald, T.J., G.L. Stephens, T.H. Vonder Haar, and D.L. Jackson, A physical retrieval of cloud liquid water over the global oceans using SSM/I observations, *J. Geophys. Res*., **98**, 18471-18488, 1993.

Gupta, S.K., W.L. Darnell, and A.C. Wilber, A parameterization for surface longwave radiation from satellite data: Recent improvements, *J. Appl. Meteor*., **31**, 1361-1367, 1992.

Hanh, C.J., S.G. Warren, J. Gordon, R.M. Chervin, and R. Jenne, Atlas of simultaneous occurrence of different cloud types over ocean. NCAR Tech. Note TN-201 + STR , 212pp, 1982.

Hanh, C.J., S.G. Warren, J. Gordon, R.M. Chervin, and R. Jenne, Atlas of simultaneous occurrence of different cloud types over land. NCAR Tech. Note TN-241 + STR , 211pp, 1984.

Hobbs, P.V., and A.L. Rangno, Ice particle concentrations in clouds, *J. Atmos. Sci.*, **42**, 2523-2549, 1985.

Hollinger, J.P., J.L. Peirce, and A. Poe, SSM/I instrument evaluation, *IEEE*, **GE-28**, 781-790, 1990.

Li, Z., and H. Le Treut, 1992: Cloud radiation feedbacks in a general circulation model and their dependence on cloud modelling assumptions, *Climate Dynamics*, **7**, 133-139.

Liao, X., W. Rossow, and D. Rind, Comparison betwen SAGE II and ISCCP high level clouds, Part I: Global and zonal mean cloud amounts, J. Geophy. Res., **100**, 1121-1135, 1995.

Liebe, H.J. An updated model for millimeter wave propagation in moist air, *Radio Sci.*, **20**, 1069-1089, 1985.

Liebe, H.J., G. Hufford, and T. Manabe, A model for the complex permittivity of water at frequencies below 1 THz, *Int. J. Infrared & Millimeter Waves*, **12**, 659-675, 1991.

Lin, B., and W.B. Rossow, Observations of cloud liquid water path over oceans: Optical and microwave remote sensing methods, *J. Geophys. Res.*, **99**, 20907-20927, 1994.

Lin, B., Observations of cloud water path and precipitation over oceans using ISCCP and SSM/I data, Ph.D. dissertation, Dept. of Geol. Sci., Columbia Univ., New York, 1995.

Lin, B., and W.B. Rossow, Seasonal variation of liquid and ice water path in non-precipitating clouds over oceans, *J. Climate*, **9**, 2890-2902, 1996.

Lin, B., and W.B. Rossow, Precipitation water path and rainfall rate estimates over oceans using special sensor microwave imager and International Satellite Cloud Climatology Project data, *J. Geophys. Res.*, **102**, 9359-9374, 1997

Lin, B., P. Minnis, B. Wielicki, D. Doelling, R. Palikonda, D. Young, and T. Uttal, Estimation of water cloud properties from satellite microwave, infrared and visible measurements in oceanic environments. II: Results. submitted to *J.Geophys. Res.*, 1997.

Liu, G., and J.A. Curry, Retrieval of precipitation from satellite microwave measurements using both emission and scattering, *J. Geophys. Res.*, **97**, 9959-9974, 1992.

Liu, G., and J.A. Curry, Determination of characteristic features of cloud liquid water from satellite microwave measurements, *J. Geophys. Res.*, **98**, 5069-5092, 1993.

McClathey, R.A., R.W. Fenn, J.E.A. Selby, F.E. Voltz, and J.S. Garing, Optical properties of the atmosphere, Air force cambridge research laboratories, AFCRL-72-0497, Environ. Res. Pap., No. 411, 1992.

Minnis, P., E. Harrison, and G. Gibson, Cloud cover over the equatorial eastern Pacific derived from July 1983 International Satellite Cloud Climatology Project data using a hybrid bispectral threshold method. *J. Geophys. Rev.*, **92**, 4051-4073, 1987.

Minnis, P., P.W. Heck D.F. Young, C.W. Fairall and J.B. Snider, Stratocumulus cloud properties derived from simultaneous satellite and island-based instrumentation during FIRE, *J. Appl. Meteorol.*, **31**, 317-339, 1992.

Minnis, P., P.W. Heck, and D.F. Young, Inference of cirrus cloud properties using satellite-observed visible and infrared radiances, Part II: Verification of theoretical cirrus radiative properties, *J. Atmos. Sci.*, **50**, 1305-1322, 1993.

Pandey, C.P., E.G. Njoku, and J.W. Waters, Inference of cloud temperature and thickness by microwave radiometery from space, *J. Clim. Appl. Meteor.*, **22**, 1894-1898, 1983.

Petty, G.W., On the response of the special sensor microwave/imager to the marine environment--Implications for atmospheric parameter retrievals, Ph.D. dissertation, Dept. of Atmos. Sci., Univ. of Washington, Seattle, 1990.

Petty,. G.W., and K.B. Katsaros, The response of the SSM/I to the marine environment. Part I: An analytic model for the atmospheric component of observed brightness temperatures, *J. Atmos. Oceanic Tech.*, **9**, 746-761, 1992.

Petty,. G.W., and K.B. Katsaros, The response of the SSM/I to the marine environment. Part II: A parameterization of the effect of the sea surface slope distribution on emission and reflection, *J. Atmos. Oceanic Tech.*, **11**, 617-628, 1994.

Poore, K., J. Wang, and W.B. Rossow, Cloud layer thicknesses from a combination of surface and upper-air observations, *J. Climate*, **8**, 550-568, 1995.

Ramanathan, V., R.D. Cess, E.F. Harrison, P. Minnis, B.R. Barkstrom, E. Ahmad and D. Hartmann, Cloud radiative forcing and climate: results from the Earth Radiation Budget Experiment, *Science*, **243**, 57-63, 1989.

Ray, P.S., Broadband complex refractive indices of ice and water, *Appl. Opt.*, **11**, 1836-1844, 1972.

Rossow, W.B., and A. Lacis, Global, seasonal cloud variations from satellite radiance measurements. Part II: Cloud properties and radiative effects, *J. Climate*, **3**, 1204-1253 1990.

Rossow, W.B., and L.C. Garder, Validation of ISCCP cloud detections, *J. Climate*, **12**, 2370-2393, 1993.

Rossow, W.B., and Y.C. Zhang, Calculation of surface and top of atmosphere radiative fluxes from physical quantities based on ISCCP datasets, Part II: Validation and first results, *J. Geophys. Res*., **100**, 1167-1197, 1995

Sassen, K., D. Starr, and T. Uttal, Mesoscale and microscale structure of cirrus clouds: Three case studies, *J. Atmos. Sci*., **46**, 371-396, 1989.

Schluessel, P., and W.J. Emery, Atmospheric water vapor over oceans from SSM/I measurements, *Int. J. Remote Sensing*, **11**, 753-766, 1990.

Sheu, R.-S., and G. Liu, Atmospheric humidity variations associated with westerly wind bursts during TOGA COARE, *J. Geophys. Res*., **100**, 25759-25768, 1995.

Smith E., A. Mugnai, H. Cooper, G. Tripoli, and X. Xiang, Foundations for statistical-physical precipitating retrieval from passive microwave satellite measurements. part I: brightness temperature properties of a time dependent cloud-radiation model. *J. App. Meteorol*., **31**, 506-531, 1992

Tian, L., and J.A. Curry, Cloud overlap statistics, *J. Geophys. Res*., **94**, 9925-9935, 1989.

Warren, S.G., Optical constants of ice from the ultraviolet to the microwave, *Applied Optics*, **23**, 1206-1255, 1984.

Warren, S.G., C.J. Hanh, and J. London, Simultaneous occurrence of different cloud types, *J. Climate Appl. Meteor*., **24**, 658-667, 1985.

Warren, S.G., C.J. Hanh, J. London, R.M. Chervin, and R.L. Jenne, Global distribution of total cloud cover and cloud type amounts over ocean, NCAR Tech. Note NCAR/TN-317+STR, 42pp, plus 170 maps, 1988.

Wielicki, B.A., R.D. Cess, M.D. King, D.A. Randall, and E.F. Harrison, Mission to planet earth: Role of clouds and radiation in climate, *Bull. Am. Meteorol. Soc*., **76**, 2125-2153, 1995.

Wilheit, T.T., A.T.C. Chang, M.S.V. Rao, E.B. Rodgers, and J.S. Theon, A satellite technique for quantitatively mapping rainfall rates over the oceans, *J. Appl. Meteorol*., **16**, 551-560, 1977.

Yeh, H.-Y.M., N. Prasad, R.A. Mack, and R.F. Adler, Aircraft microwave observations and simulations of deep convection from 18 to 183 GHz. Part II: Model Results, *J. Atmos. Oceanic Tech*., **7**, 392-410, 1990.

Table 1 Cloud heights for the four climate profiles

	Low	lower middle	upper middle	high
Tropics	2	4	7	10.5
Midlat. Summer	2	4	7	10.5
Midlat. Winter	2	4	6	7.5
US Standard	2	4	6	8.5

Note: This study only simulates microwave radiation for water clouds with 0.5km thickness in four different levels: low, lower middle, upper middle and high, as indicated in the table. The units for cloud heights are km.

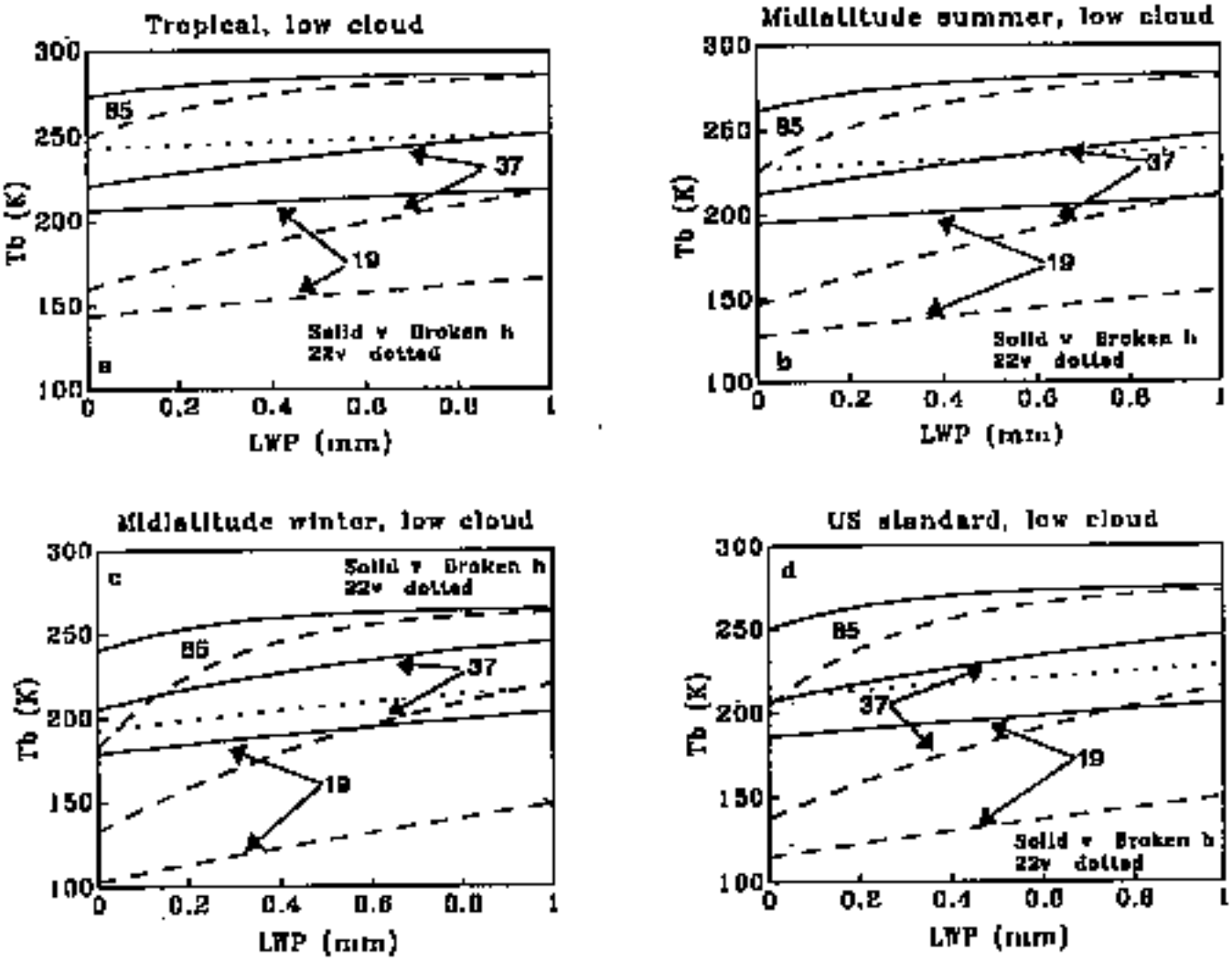

Figure 1

Figure 1. Simulated SSM/I brightness temperatures for low-level liquid water clouds in various atmospheres.

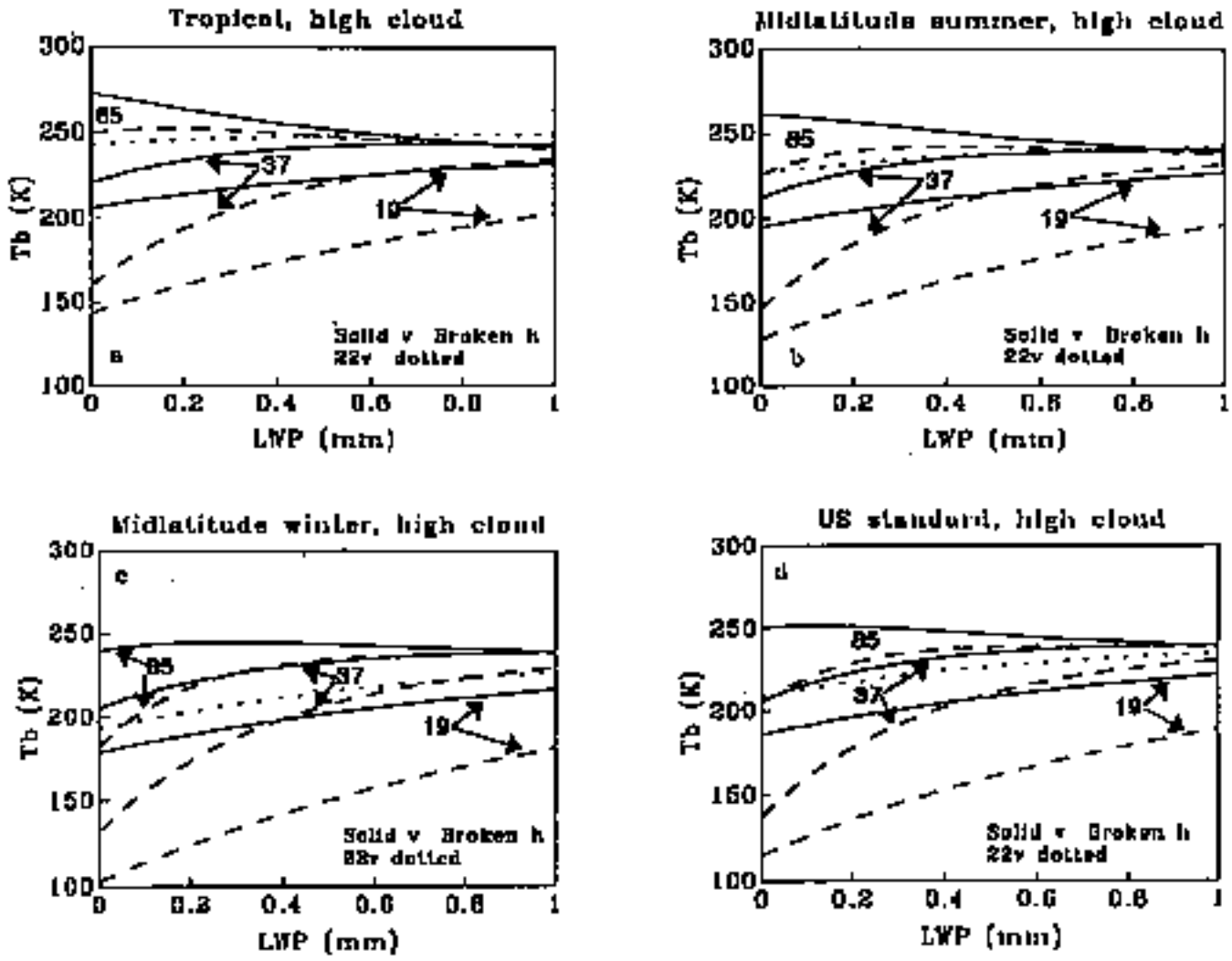

Figure 2

Figure 2. Same as Figure 1, except for high-level liquid water clouds.

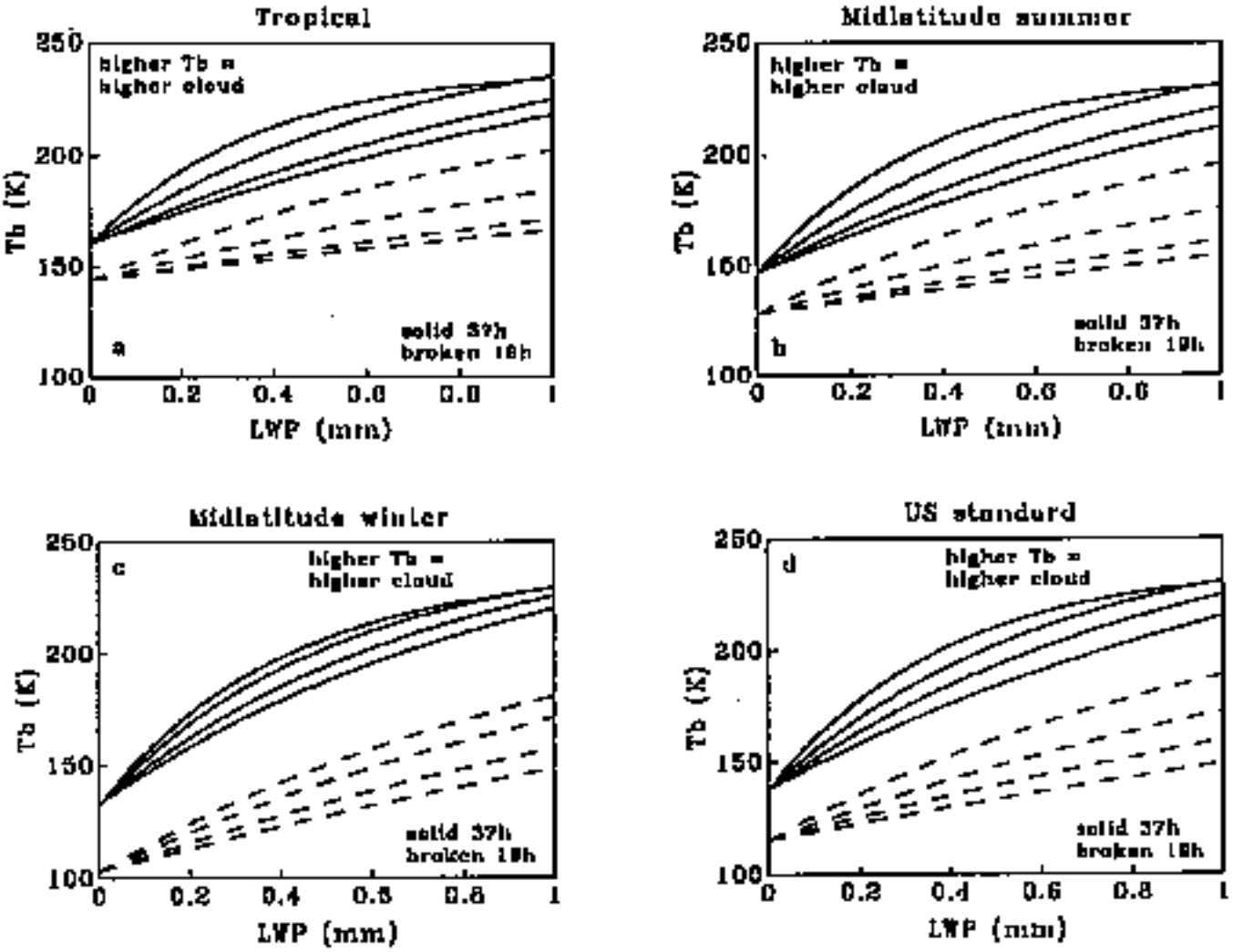

Figure 3

Figure 3. Simulated horizontally polarized brightness temperatures of SSM/I at 37 and 19 GHz for various atmospheric profiles. The four curves for each frequency represent *Tb* for high, upper middle, lower middle, and low-level liquid water clouds. *Tb* increase with increasing altitude.

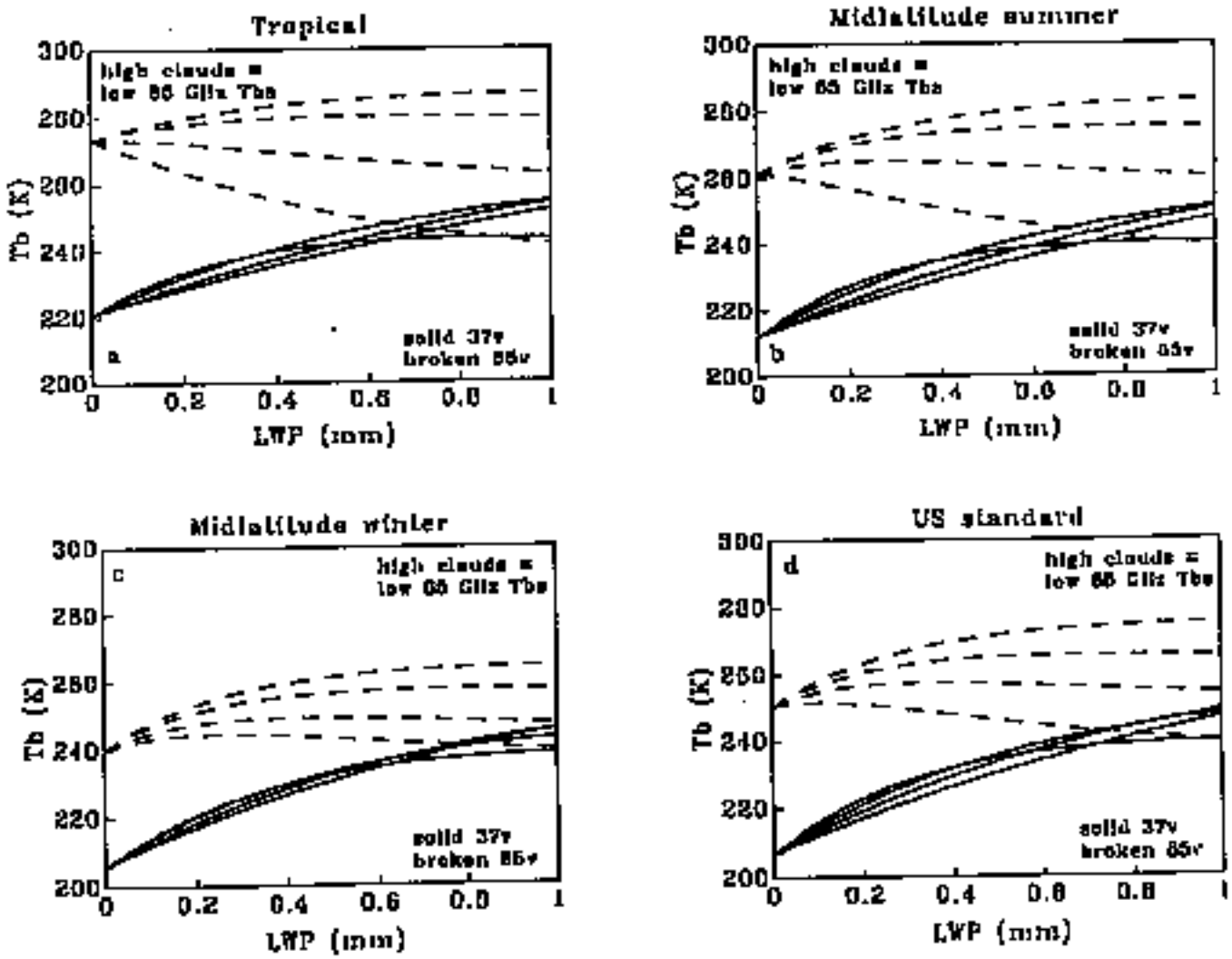

Figure 4

Figure 4. Same as Figure 3, but for 85 and 37 GHz vertically polarized *Tb*s. For 85 GHz, *Tb* decreases with increasing altitude.

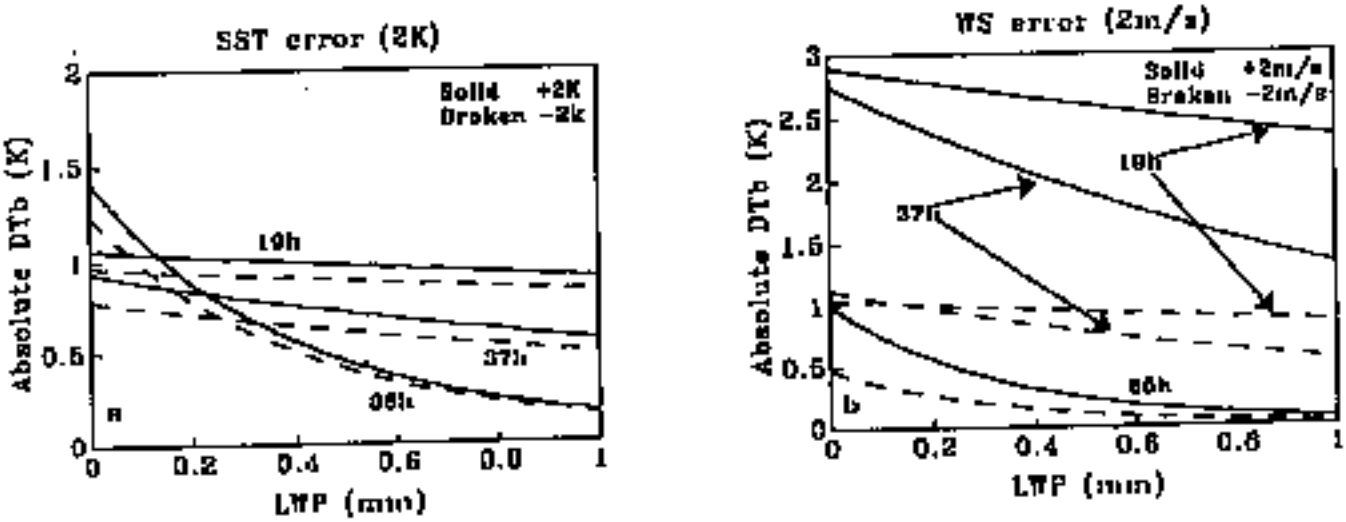

Figure 5

Figure 5. Simulated absolute values of uncertainty for 19, 37, and 85 GHz horizontally polarized brightness temperatuires due to errors of ± 2K SST(a) and ± 2 m/s near−sea surface windspeed (b) for lower middle−level clouds in a midlatitude summer profile.

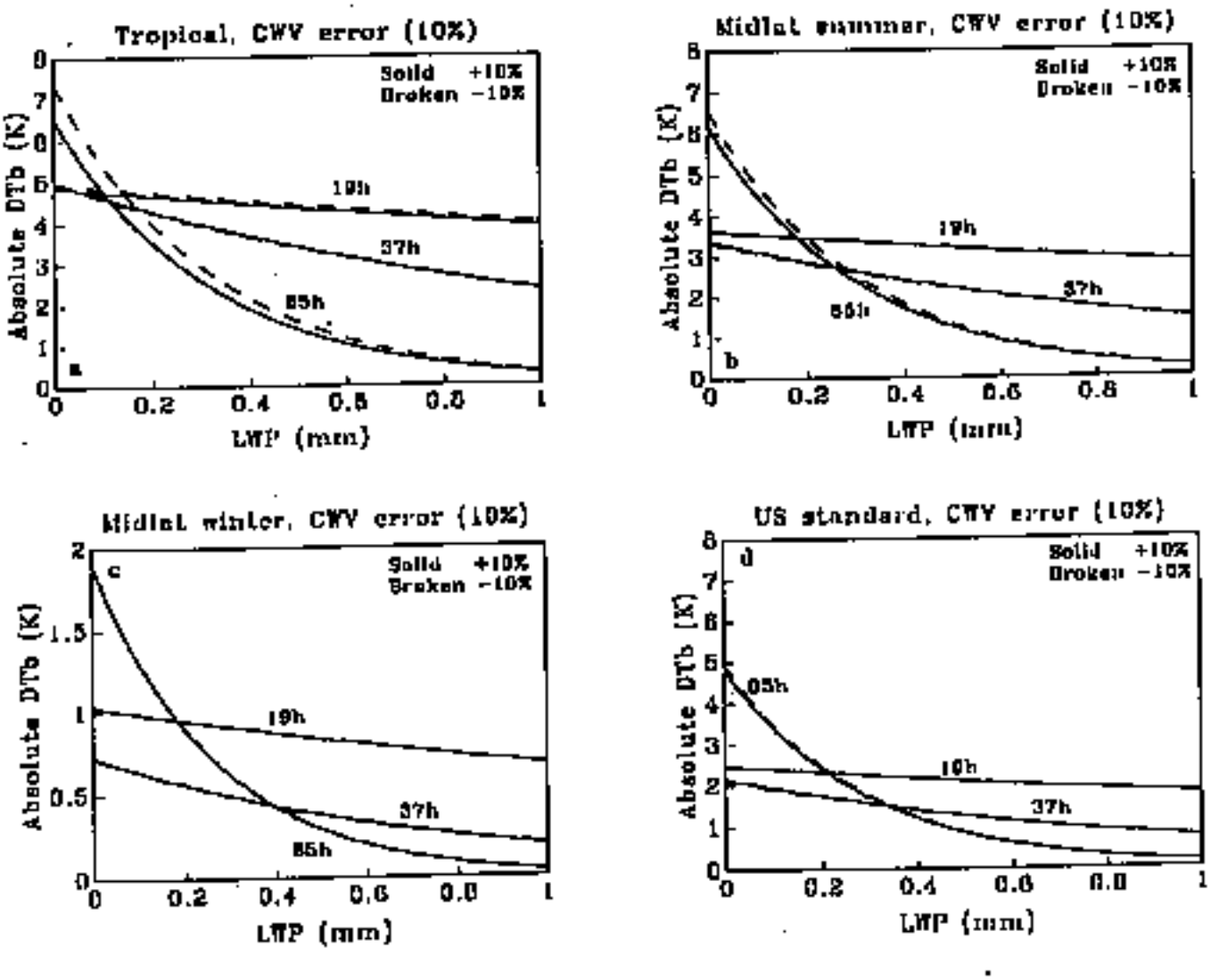

Figure 6

Figure 6. Same as Figure 5, except with ± 10% *CWV* uncertainty for all four atmospheres.

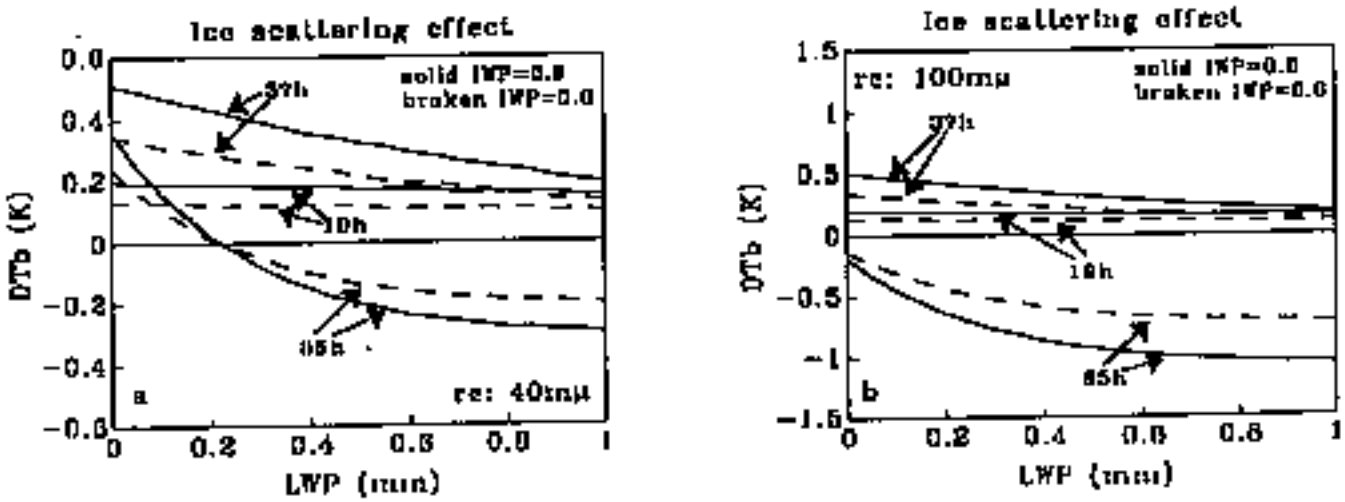

Figure 7

Figure 7. Simulated horizontally polarized *Tb*s at 19, 37, and 85 GHz for 40−mm (a) and 100−mm (b) radius ice particles.

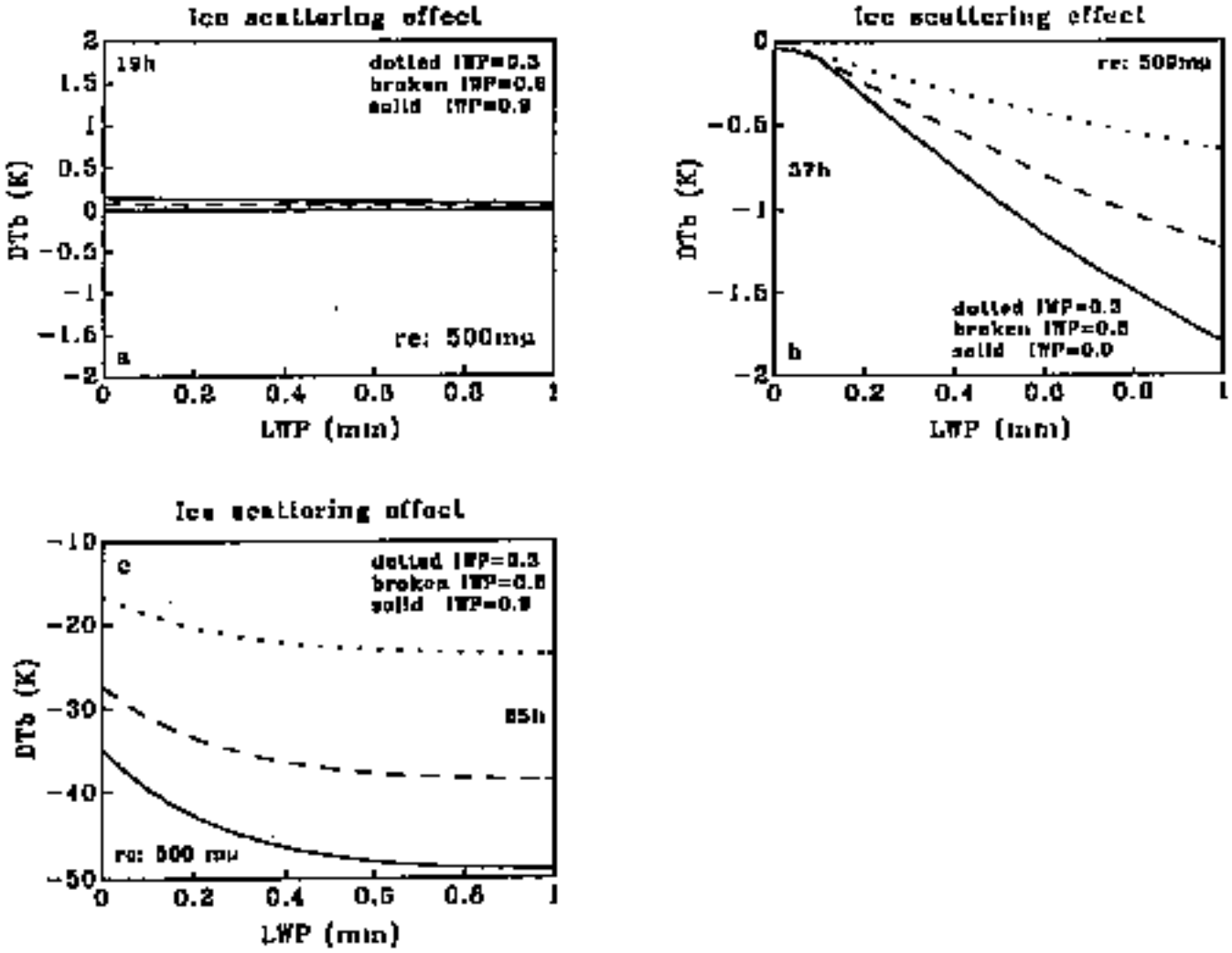

Figure 8

Figure 8. Same as figure 7, but with 500−mm radius ice particles for a) 19 GHz, b) 37 GHz, and c) 85 GHz.

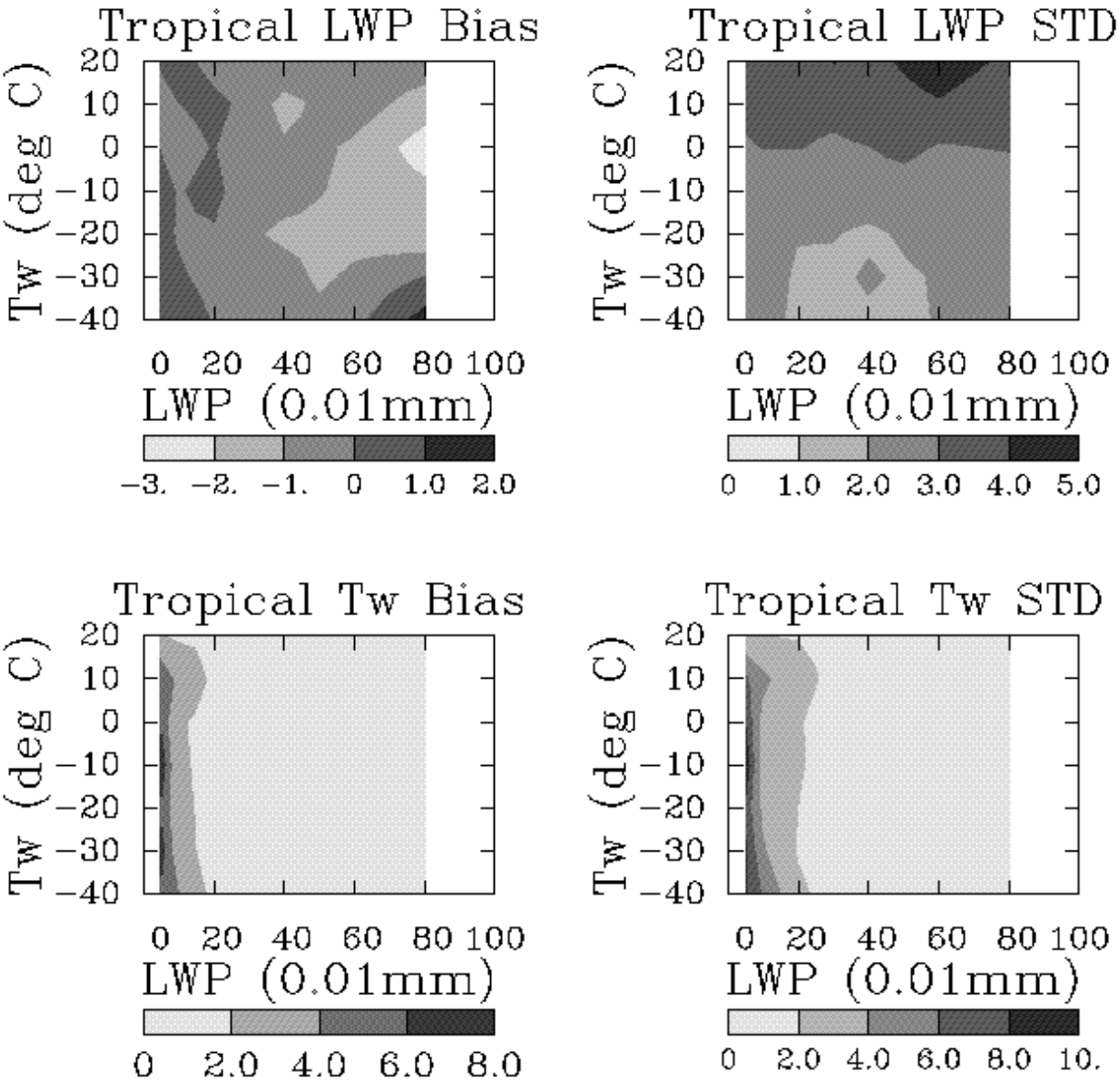

Figure 9. The simulated bias (left panels) and standard deviation (right panels) of *LWP* (upper panels in 0.01 mm) and *Tw* (lower panels in deg C) for tropical climates.

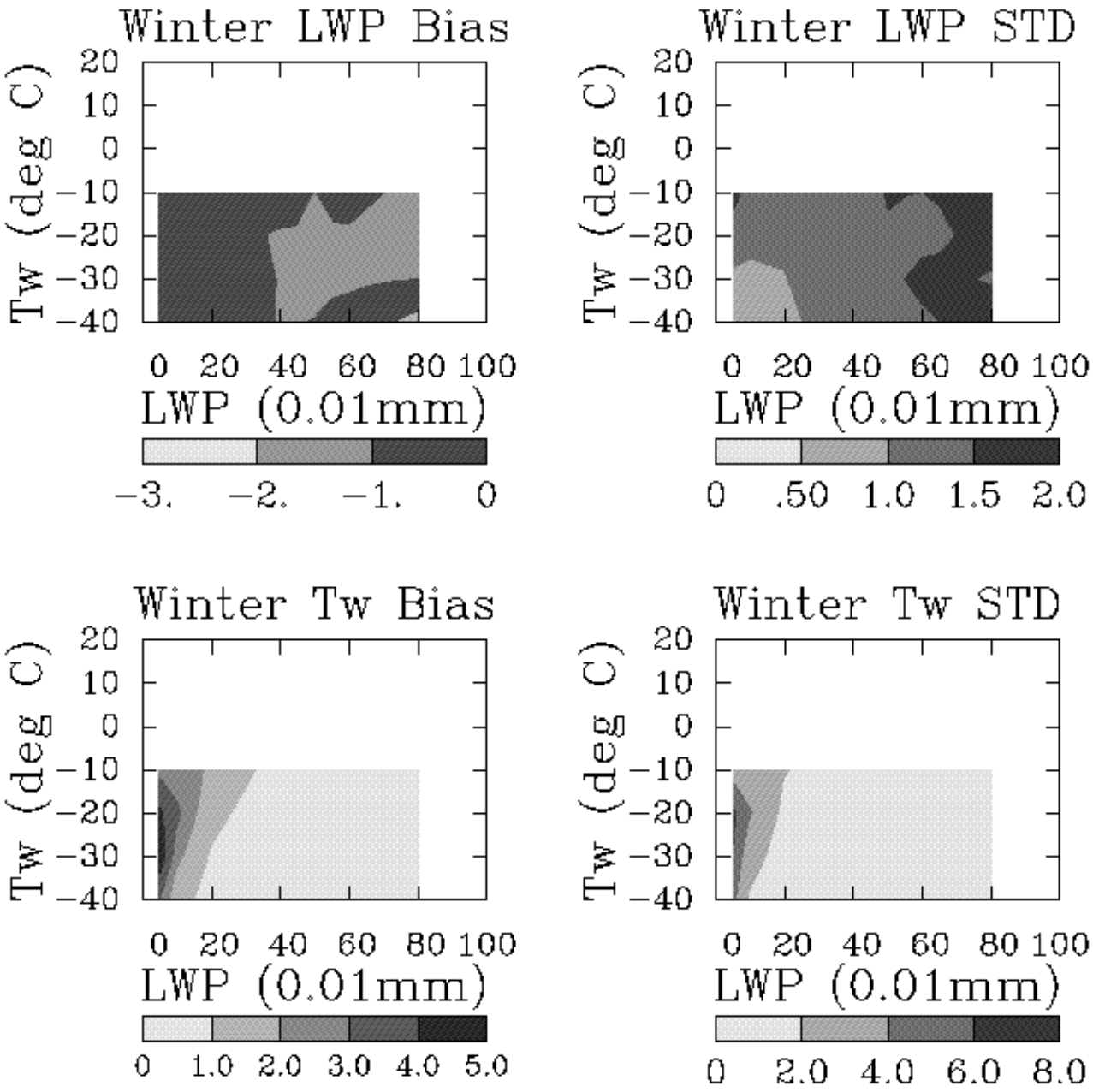

Figure 10. Same as Figure 9, but for midlatitude winter.

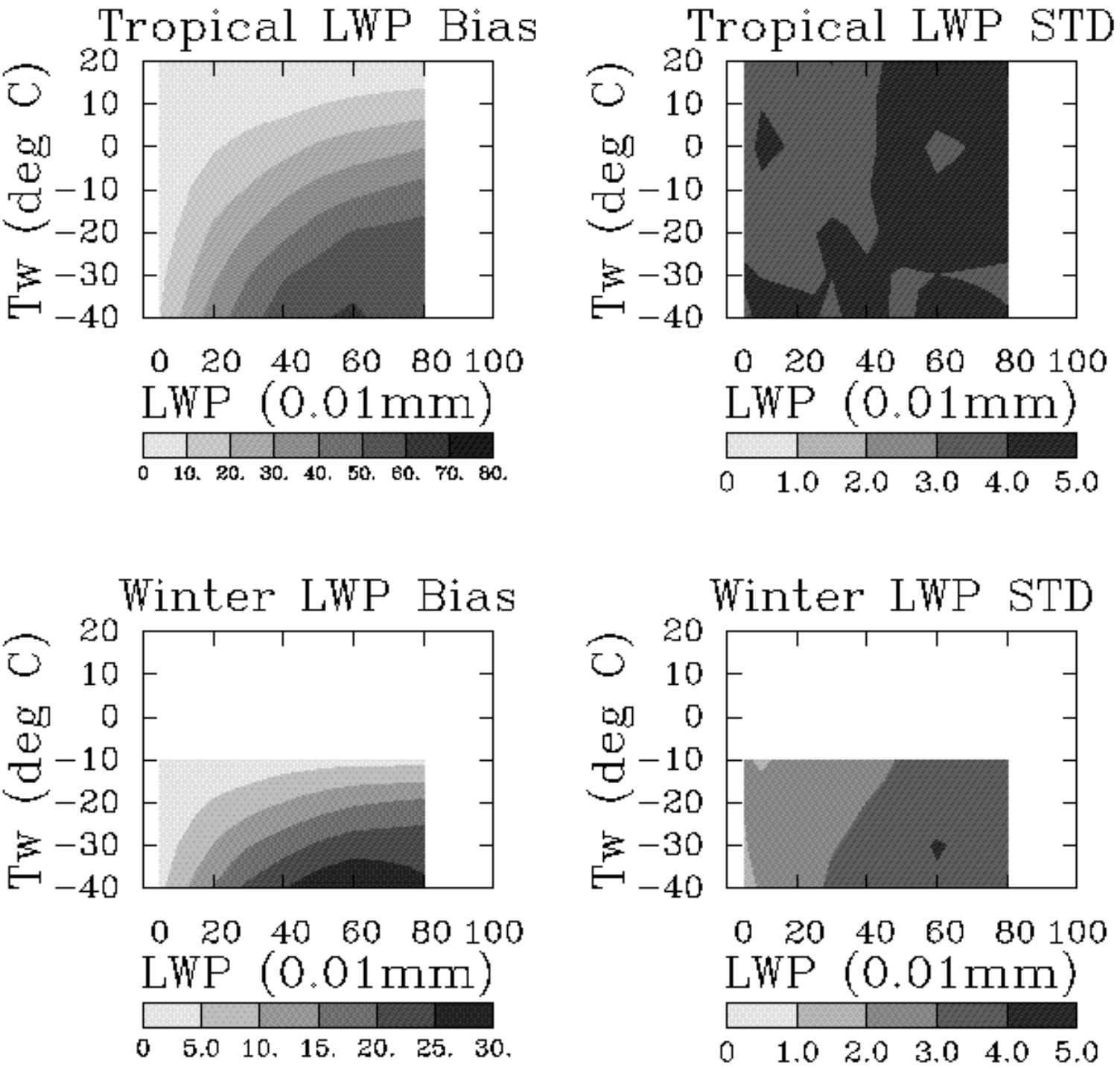

Figure 11. Same as Figure 9, but for the bias and standard deviation of *LWP* estimated from the method assuming *Tw* = *SST* − 6K.

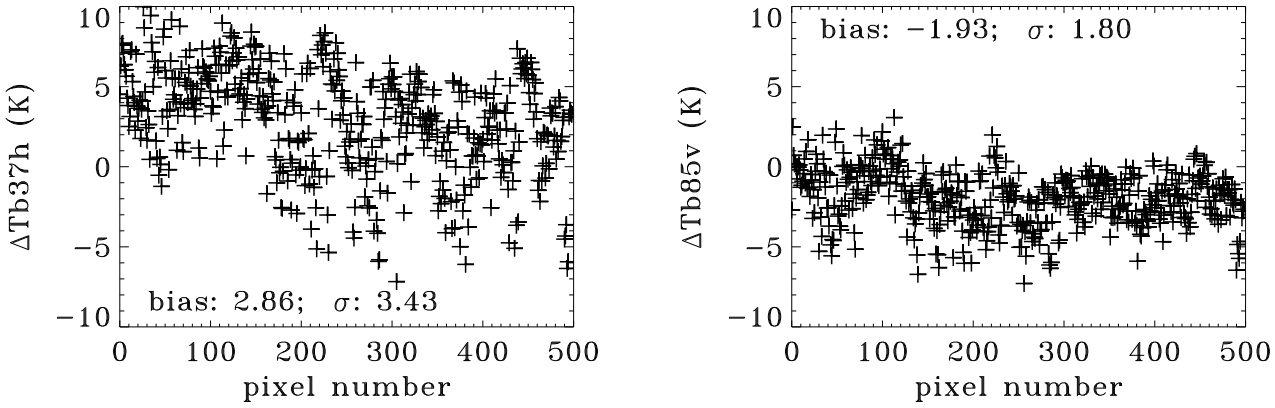

Figure 12. Brightness temperature differences (in K) between SSM/I measurements and simulations at 37h (left panel) and 85v (right panel) channels for clear-sky cases.

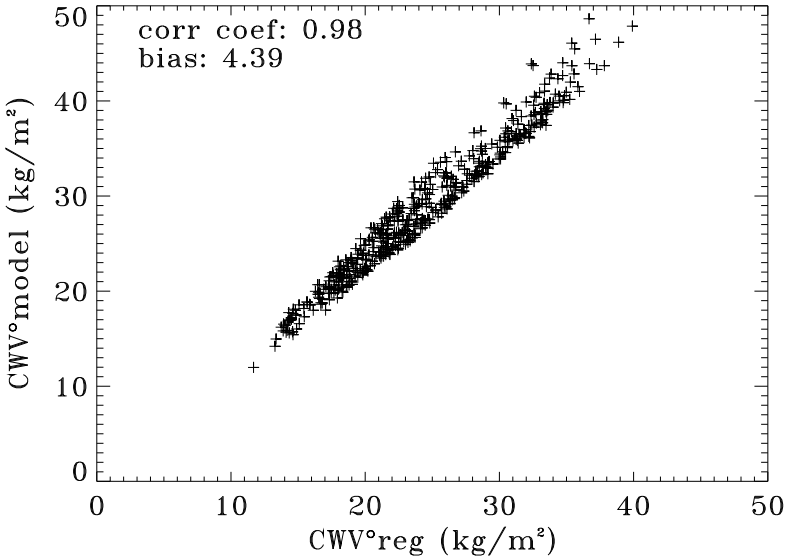

Figure 13. CWV (in kg/m2) comparison between current model estimates and the retrievals using the Schluessel and Emery [1990] method.